THE JOURNAL OF PHYSICAL CHEMISTRY C

Subscriber access provided by DUESSELDORF LIBRARIES

Article

Orbital Overlap Effects in Electron Transfer Reactions Across a Metal Nanowire/Electrolyte Solution Interface

Renat Ravilevich Nazmutdinov, Alexander Berezin, Germán José Soldano, and Wolfgang Schmickler

J. Phys. Chem. C, **Just Accepted Manuscript** • DOI: 10.1021/jp400037g • Publication Date (Web): 30 May 2013

Downloaded from http://pubs.acs.org on June 15, 2013

Just Accepted

"Just Accepted" manuscripts have been peer-reviewed and accepted for publication. They are posted online prior to technical editing, formatting for publication and author proofing. The American Chemical Society provides "Just Accepted" as a free service to the research community to expedite the dissemination of scientific material as soon as possible after acceptance. "Just Accepted" manuscripts appear in full in PDF format accompanied by an HTML abstract. "Just Accepted" manuscripts have been fully peer reviewed, but should not be considered the official version of record. They are accessible to all readers and citable by the Digital Object Identifier (DOI®). "Just Accepted" is an optional service offered to authors. Therefore, the "Just Accepted" Web site may not include all articles that will be published in the journal. After a manuscript is technically edited and formatted, it will be removed from the "Just Accepted" Web site and published as an ASAP article. Note that technical editing may introduce minor changes to the manuscript text and/or graphics which could affect content, and all legal disclaimers and ethical guidelines that apply to the journal pertain. ACS cannot be held responsible for errors or consequences arising from the use of information contained in these "Just Accepted" manuscripts.

ACS Publications
High quality. High impact.

The Journal of Physical Chemistry C is published by the American Chemical Society. 1155 Sixteenth Street N.W., Washington, DC 20036
Published by American Chemical Society. Copyright © American Chemical Society. However, no copyright claim is made to original U.S. Government works, or works produced by employees of any Commonwealth realm Crown government in the course of their duties.

Orbital Overlap Effects in Electron Transfer Reactions across a Metal Nanowire/Electrolyte Solution Interface

[(a)*]Renat R. Nazmutdinov, [(a)]Alexander S. Berezin, [(b)]Germán Soldano and [(b)]Wolfgang Schmickler

[(a)]Kazan National Research Technological University, 420015 Kazan, Republic of Tatarstan, Russia

[(b)]Institute of theoretical chemistry, University of Ulm, D-86069 Ulm, Germany

Abstract

In this communication we report on calculations of the orbital overlap between Fe(III) and Cr(III) aquacomplexes and different electrode surfaces: Cu(111), Ag (111), Au(111), Pt(111), and corresponding monoatomic wires. The electronic structure of the monocrystalline surfaces and nanowires are described in terms of the electronic spillover and density of electronic states at the Fermi level obtained from periodic Density Functional Theory (DFT) calculations. The transmission coefficients (κ) characterizing the first stage of outer-sphere electron transfer for the reduction of aquacomplexes are calculated on the basis of Landau-Zener theory as a function of electrode – reactant separation; the electronic transmission coefficients for the $[Cr(H_2O)_6]^{3+/2+}$ redox couple were found to be smaller than those for $[Fe(H_2O)_6]^{3+/2+}$. Two different intervals can be clearly distinguished for Cu, Au and Pt: "a catalytic region", where κ(wire) > κ(Me slab) and "an inhibition region", where κ(wire) < κ(Me slab). A similar behaviour exhibits the coupling constant estimated for a hydrogen atom adsorbed at the Au(111) surface and the Au monoatomic wire. These effects originate from some specific features of electronic density profile for metal nanowires: at short distances the electronic density of nanowires is higher compared with the (111) metal surfaces, while at larger separations it decreases more sharply.

Key words: metal nanowire; electron transfer; electronic transmission coefficient; density functional theory; Au, Cu, Ag, Pt electrodes; Cr(III) and Fe(III) aquacomplexes.

*corresponding author, Tel: +7(843)231-89-83; E-mail: nazmutdi@mail.ru

I. Introduction

Conducting nanowires and nanotubes in contact with an electrolyte solution can be regarded as promising, important and challenging electrochemical systems. Recently, a few attempts have been made to describe theoretically the structure of such interfaces[1-5]. The electric double layer (EDL) at a conducting nanocylinder/electrolyte solution interface was modeled by using Gouy-Chapmen theory[1,2,3] and classical molecular dynamics simulations[4,5]. The charge transfer across nanowire (nanotube)/aqueous solution interface was addressed in Refs.[3, 6-9] on the basis of quantum mechanical theory[10, 11]. Some qualitatively interesting features were predicted for the $[Fe(CN)_6]^{3-/4-}$ redox couple[3] (electrostatic catalysis, inverted Arrhenius plot) and the reduction of peroxodisulphate anion[9] (disappearance of a "pit" in current – voltage curves observed in diluted supporting electrolyte solutions). Sizable catalytic effects were predicted when considering the hydrogen evolution on different metal nanowires[7, 8]. At the same time the orbital overlap between reactant and electrode of nanosize was investigated only in the strong coupling limit (adiabatic electron transfer)[7, 8]. The electronic transmission coefficient for redox couples in non-adiabatic (weak coupling) limit at a nanowire (nanotube) electrodes have not been calculated systematically or properly analyzed; the role of the electrode material was not elucidated as well. In this work we address the orbital overlap effect for $Fe^{3+/2+}$ and $Cr^{3+/2+}$ redox couples for four different metal electrode (Ag, Au, Cu and Pt) using model approaches developed previously. The metals are represented by both (111) faces of monocrystals and monoatomic wires. Electron transfer for these redox systems has outer-sphere character and is expected to be non-adiabatic. As reduction (oxidation) proceeds in this case at low electrode overvoltages (in contrast to $[Fe(CN)_6]^{3-/4-}$ and the peroxodisulphate anion), the electrical double layer effects do not play an important role and can be neglected. These features of the $Fe^{3+/2+}$ and $Cr^{3+/2+}$ redox couples allow considering them as a convenient model system.

This paper is organized as follows: Details of model calculations are described in Section II and the results are reported in Section III. Some concluding remarks are listed in Section IV.

II. Model and computational details

The electronic transmission coefficient (κ_e) was treated in the framework of the Landau-Zener theory[10]:

$$\kappa_e = 1 - \exp(-2\pi\gamma_e), \quad (1)$$

where $2\pi\gamma_e$ is the Landau-Zener (LZ) factor.

Eq.1 is true for two crossing free energy surfaces along the reaction coordinate when considering only direct trajectories. If both direct and backward trajectories are addressed, one must take into account the denominator $1-\frac{1}{2}\exp(-2\pi\gamma_e)$. The latter, strictly speaking is not correct for a heterogeneous electron transfer, because in this case we have to deal with a random rambling through a network formed by the crossing points of a manifold of free energy surfaces[11]. That is why a simple equation (1) was used in further calculations.

When intramolecular reorganization can be described in terms of linear response, γ_e at small electrode overvoltages is calculated as follows:

$$\gamma_e = \frac{\rho(\varepsilon_F)}{\hbar\omega_{eff}}\sqrt{\frac{\pi k_B T}{\lambda}}\left(\frac{\Delta E_e}{2}\right)^2, \quad (2)$$

where ΔE_e is the resonance splitting of the reaction free energy surfaces; λ is the total reorganization energy; ω_{eff} is the effective frequency of polar medium (10^{13} Hz)[10]; $\rho(\varepsilon_F)$ is the density of electronic states of electrode at the Fermi level.

In eq.(2) the LZ factor is directly proportional to the density of electronic states but this is true only in the region of small electrode – reactant electronic coupling (non-adiabatic limit of electron transfer). So far no exact solution is known for the wide region of electronic coupling,

although some useful results can be obtained numerically using Monte Carlo simulations[11] (see also Supporting Information, Fig.1S).

Below we dwell upon a quantum chemical model to calculate ΔE_e. Let us consider the electron exchange between a metal electrode and a reactant. If the electron is located on the metal electrode (initial state) the total Hamiltonian can be represented as follows,

$$\hat{H} = \hat{H}_i^{(0)} + \hat{V}_f, \tag{3}$$

and $\hat{H}_i^{(0)}$ is the Hamiltonian of the electron in initial state:

$$\hat{H}_i^{(0)}\psi_i = \varepsilon_i\psi_i, \tag{4}$$

where ψ_i is a one-electron wave function of the metal; the eigenvalue ε_i is the electron energy in initial state.

The operator $\hat{V}_f$ in eq.3 describes the influence of acceptor (reactant) on the electron in initial state. On the contrary, if the electron is located on the reactant (final state) the total Hamiltonian takes the form:

$$\hat{H} = \hat{H}_f^{(0)} + \hat{V}_i, \tag{5}$$

and $\hat{H}_f^{(0)}$ is the Hamiltonian of the electron in final state:

$$\hat{H}_f^{(0)}\psi_f = \varepsilon_f\psi_f, \tag{6}$$

where ψ_f is a one-electron wave function of the reduced reactant; the eigenvalue ε_f is the electron energy in final state.

In this case the operator $\hat{V}_i$ describes the influence of donor (metal electrode). Then we have

$$\frac{\Delta E_e}{2} = \frac{\langle \psi_i | \hat{H} | \psi_f \rangle - \langle \psi_i | \hat{H} | \psi_i \rangle \langle \psi_i | \psi_f \rangle}{1 - \langle \psi_i | \psi_f \rangle^2}, \quad (7)$$

where $\langle \psi_i | \hat{H} | \psi_f \rangle = \int \psi_i \hat{H} \psi_f d\Omega$, $\langle \psi_i | \hat{H} | \psi_i \rangle = \int \psi_i \hat{H} \psi_i d\Omega$ and $\langle \psi_i | \psi_f \rangle = \int \psi_i \psi_i d\Omega$.

One can write neglecting the $\langle \psi_i | \psi_f \rangle^2$ term♣:

$$\frac{\Delta E_e}{2} = \langle \psi_i | \hat{H} | \psi_f \rangle - \langle \psi_i | \hat{H} | \psi_i \rangle \langle \psi_i | \psi_f \rangle. \quad (8)$$

Due to the Hermitian character of the electronic Hamiltonian and normalization conditions of the wave functions ψ_i and ψ_f the following equations are to be fulfilled:

$$\langle \psi_i | \hat{H} | \psi_f \rangle = \langle \psi_f | \hat{H} | \psi_i \rangle \quad (9)$$

and

$$\langle \psi_i | \psi_i \rangle = \langle \psi_f | \psi_f \rangle = 1. \quad (10)$$

Then we can recast eq.8 in the form#

♣ As ψ_i is normalized to the metal volume V_{Me}, the $\langle \psi_i | \psi_f \rangle^2$ term is proportional to $1/V_{Me}$ and, therefore, tend to zero for a semi-infinite metal (infinite metal wire)

It is evident from eq.14 that $\langle \psi_i | \hat{V}_f | \psi_f \rangle = \langle \psi_f | \hat{V}_f | \psi_i \rangle$.

$$\frac{\Delta E_e}{2} = \langle \psi_f | \hat{H}_i^{(0)} | \psi_i \rangle + \langle \psi_f | \hat{V}_f | \psi_i \rangle - \langle \psi_i | \hat{H}_i^{(0)} | \psi_i \rangle \langle \psi_i | \psi_f \rangle - \langle \psi_i | \hat{V}_f | \psi_i \rangle \langle \psi_i | \psi_f \rangle =$$

$$\varepsilon_i \langle \psi_i | \psi_f \rangle + \langle \psi_f | \hat{V}_f | \psi_i \rangle - \varepsilon_i \langle \psi_i | \psi_f \rangle - \langle \psi_i | \hat{V}_f | \psi_i \rangle \langle \psi_i | \psi_f \rangle =$$

$$\langle \psi_i | \hat{V}_f | \psi_f \rangle - \langle \psi_i | \hat{V}_f | \psi_i \rangle \langle \psi_i | \psi_f \rangle . \quad (11)$$

In calculations of κ_e for the heterogeneous electron transfer, on the other hand, we have to deal with the product $\rho(\varepsilon_F)\left(\frac{\Delta E_e}{2}\right)^2$ (see eq.2):

$$\rho(\varepsilon_F)\left(\frac{\Delta E_e}{2}\right)^2 = \rho(\varepsilon_F)\langle \psi_i | V_f | \psi_f \rangle^2 - 2\rho(\varepsilon_F)\langle \psi_i | V_f | \psi_f \rangle \langle \psi_i | V_f | \psi_i \rangle \langle \psi_i | \psi_f \rangle +$$

$$\rho(\varepsilon_F)\left(\langle \psi_i | V_f | \psi_i \rangle \langle \psi_i | \psi_f \rangle\right)^2 . \quad (12)$$

Note that the wave function ψ_i is normalized to the metal volume V_{Me}. For a semi-infinite metal (infinite metal wire) both $\rho(\varepsilon_F)$ and V_{Me} tend to infinity; their ratio $\rho(\varepsilon_F)/V_{Me}$, however, is a finite quantity which is assumed in eq.2. It is easy to see that the second and the third terms in eq.12 are vanishing (they are proportional to $\rho(\varepsilon_F)/V_{Me}^2$ and $\rho(\varepsilon_F)/V_{Me}^3$, respectively, see also Ref.[22]).

Finally we have

$$\frac{\Delta E_e}{2} = V_{if} = \langle \psi_i | V_f | \psi_f \rangle . \quad (13)$$

It was already mentioned above that the matrix element V_{if} can be calculated in the framework of the perturbation theory. In the Hartree-Fock theory the perturbation operator V_f consists of Coulomb and exchange terms. The last term is noticeable only for short metal – reactant

separations and can be neglected. The Coulomb term can be defined as a molecular potential induced by the reactant in oxidized state[&]:

$$V_f(\vec{r}) = \sum_j \frac{q_j}{\left|\vec{R}_j - \vec{r}\right|}, \qquad (14)$$

where q_j are the atomic charges calculated using the ChelpG scheme[12]; the radius-vectors $\vec{R}_j$ describe the position of the atoms.

Models to calculate the electronic coupling matrix element for electron transfer across metal/liquid and semi-conductor/liquid interfaces were developed previously by Marcus et al[13-15].

The calculations of the geometry and electronic structure of $[Fe(H_2O)_6]^{3+/2+}$ and $[Cr(H_2O)_6]^{3+/2+}$ were performed at the DFT level with the hybrid functional B3LYP as implemented in the *Gaussian* 03 program suite[16]. A basis set of DZ quality was employed to describe the valence electrons of Fe atom, whereas the effect of inner electrons was included in a relativistic Effective Core Potential (ECP) developed by Hay and Wadt (LanL2)[16]. The standard 6-31g basis set augmented by polarization functions was used to describe the electrons in the O and H atoms. The unrestricted DFT formalism was employed to describe the open-shell systems. The geometry of the aquacomplexes in oxidized and reduced states was optimized without symmetry restrictions. The periodical DFT calculations have been performed with the *Dacapo* code[17] for the Ag, Au, Cu and Pt electrodes in two different configurations: Me(111) metal surface (six-layer slab) and a monoatomic wire. The Brillouin zone integration was done using the Monkhorst-Pack grid[18]; the PW91-GGA approximation to the exchange-correlation energy was employed[19]. Nuclei and core electrons have been described by ultrasoft pseudopotentials[20]. Other pertinent details of the calculations can be found in Refs.[7, 8]. For both the Me(111) and the Me monoatomic wire we calculated the density of electronic states $\rho(\varepsilon)$ and the electronic density profile along the surface normal $n(x)$ (averaged over

[&] For the sake of simplicity we did not take into account the screening of the molecular potential by fast solvent modes, although this effect can be readily addressed [9].

the surface). Outside the metal (i.e. in the most important overlap region) the electronic density was fitted by an exponential decay:

$$n(x) = |\psi_i(x)|^2 = n_0 \exp(-\beta x). \quad (15)$$

Then the effective one-electron orbital of a metal electrode can be obtained directly from eq.15. This way to construct the orbital of a metal electrode resembles to some extent an approach developed previously in the work[21]. In calculations of the matrix element V_{if} the highest occupied β-molecular orbital of $[Fe(H_2O)_6]^{2+}$ and α - molecular orbital of $[Cr(H_2O)_6]^{2+}$ were used for ψ_f; the geometry of the aquacomplexes was fixed at initial (oxidized) state in an assumed rough Condon approximation[10]).

In the present work we have improved the method for the calculation of V_{if} developed previously for a reactant near a plain electrode surface (see pertinent details in Refs.[9, 22, 23] and adapted it to electrodes of cylindrical form with arbitrary radius *a*. The integration was performed over the 3D half-space ($x \geq 0$) for the Me(111) surfaces and over the whole space ($x \geq a$) for the monoatomic wires. The conditions $x = 0$ and $x = a$ correspond to the electrode "edge"; the atomic radii of the metals were taken as the *a* values in our calculations. The influence of the electronic in the half-space $x \leq 0$ (plane electrodes) and $0 \leq x <$ a (cylinders) was found to be negligibly small. The numerical calculations were performed using an original code written with the program package "*Matlab* R2009b".

III. Results and discussion

Parameters characterizing the electronic structure of metal electrodes are compiled in the Table. It can be seen that the parameter describing the electronic density decay (β) increases in the row Pt < Ag =Au < Cu; our results for Ag(111) and Au(111) predict a more noticeable decay for

electronic density as predicted from the jellium model[21], although the differences are not large. The β values calculated for the wires exceed those obtained for the Me(111) surface, i.e electronic density near the monoatomic wires decays more strongly; partially, this is caused by a geometric effect: cylindrical geometry on the wires compared to one-dimensional decay on the plane surfaces. In contrast, for all metals the parameter n_0 describing electronic density at the surface "edge" is significantly smaller for the slabs than for the wires. The density of electronic states at the Fermi level for Pt was calculated by Gosavi and Marcus[14, 15] as 7.6 times as larger as for Au. The ratio of $\rho(\varepsilon_F)$ for the same metals found by us (6.2) is a good agreement with this conclusion (see Table), but for both metals our values are significantly smaller. For Cu and Au the $\rho(\varepsilon_F)$ values characterizing the metal wires noticeably exceed those for the metal slabs. Pt and Ag reveal nearly the same $\rho(\varepsilon_F)$ both for Me(111) and for the wires. Such conspicuous features of the electronic structure of the metals slabs and wires should affect the orbital overlap effects and hence electron transfer kinetics.

Table. Density of electronic states at the Fermi level*, $\rho(\varepsilon_F)$ and two parameters describing the exponential fit of the electronic density (see eq.15) calculated for the Me(111) surfaces and nonoatomic metal wires (Me=Ag, Au, Cu, Pt).

		Ag	Au	Cu	Pt
$\rho(\varepsilon_F)$ /eV^{-1} atom^{-1}	Me(111)	0.148	0.165 (0.29)**	0.175	1.03 (2.2)**
	wire	0.2	0.51	0.5	0.8
β /a.u.$^{-1}$	Me(111)	1.396 (1.23)***	1.39 (1.22)***	1.842	1.28
	wire	1.426	1.738	2.303	1.594
n_0**** /a.u.$^{-3}$	Me(111)	0.09	0.102	0.146	0.081
	wire	0.217	0.427	0.63	0.306

*normalized to the number of atoms in the unit cell: 6 atoms for Me(111) and 1 atom for the mono-atomic wire.

**calculated in Refs.[14, 15] using a tight binding approach and the extended Hückel method.

***calculated on the basis of the jellium model for the metal surface[24].

****normalized to the number of electrons in the unit cell.

The total spin numbers (S) are 5/2 and 2 for $[Fe(H_2O)_6]^{3+}$ and $[Fe(H_2O)_6]^{3+}$, respectively. In turn, S = 3/2 and 2 for the Cr(III) and Cr(II) aquacomplexes. The corrsponding $<S^2>$ values were computed to be 8.7553 (6.0033) and 3.7593(6.0035) for the Fe(III)(Fe(II)) and Cr(III)(Cr(II)) aquacomplexes. Resting on the results of quantum chemical calculations we have estimated the intramolecular contributions to the total reorganization energy, λ_{in} = 0.34 eV ($Fe^{3+/2+}$) and 0.77 eV ($Cr^{3+/2+}$), which are close to the estimates reported previously by Rosso and Rustad[25]. When calculating the electronic transmission coefficient we used for simplicity the λ_{in} values by averaging the intramolecular reorganization energies for reduction and oxidation processes[26]. The reorganization of coordination shell for $Cr^{3+/2+}$ is more significant due to the Jahn-Teller distortions in the $[Cr(H_2O)_6]^{2+}$ aquacomplex. The solvent reorganization energy was calculated to be 0.87 eV at x =0.65 nm (see pertinent technical details in Ref.[23]).

Three different orientations of the Fe(III) ad Cr(III) aquacomplexes relative to the metal (111) surface and the wires were considered: (a) "apex", (b) "face" and (c, d) "ridge" (see Fig.1). The orientation (a) results in a very small orbital overlap due to symmetry reasons and was excluded from further analysis. The orientations (b) and (c) are characterized nearly by the same orbital overlap. In what follows we report the results only for the "ridge" orientation. Since for the both aquacomplexes the acceptor quasi t_{2g} and e_g molecular orbitals are nearly degenerated, in general they must be considered with some averaging technique in calculations of kinetic parameters. This issue was investigated in detail for $[Fe(H_2O)_6]^{3+}$ (see Supporting Information). For all three orientations only one half-occupied t_{2g} orbital of the aquacomplex plays the most important role in the electronic coupling and, therefore, mainly contributes to κ_e (Fig.2S). The contributions from the other two t_{2g} orbitals are significantly smaller and can be neglected.

The electronic transmission coefficients as a function of the reactant – metal slab separation x are plotted in Fig.2a. It can be seen that for all four metals electron transfer to the $[Fe(H_2O)_6]^{3+}$ aquacomplex is non-adiabatic at $x \geq 0.65$ nm. This distance of the closest approach presumes a monolayer of solvent molecules between the aquacomplex and the electrode surface. Previously the

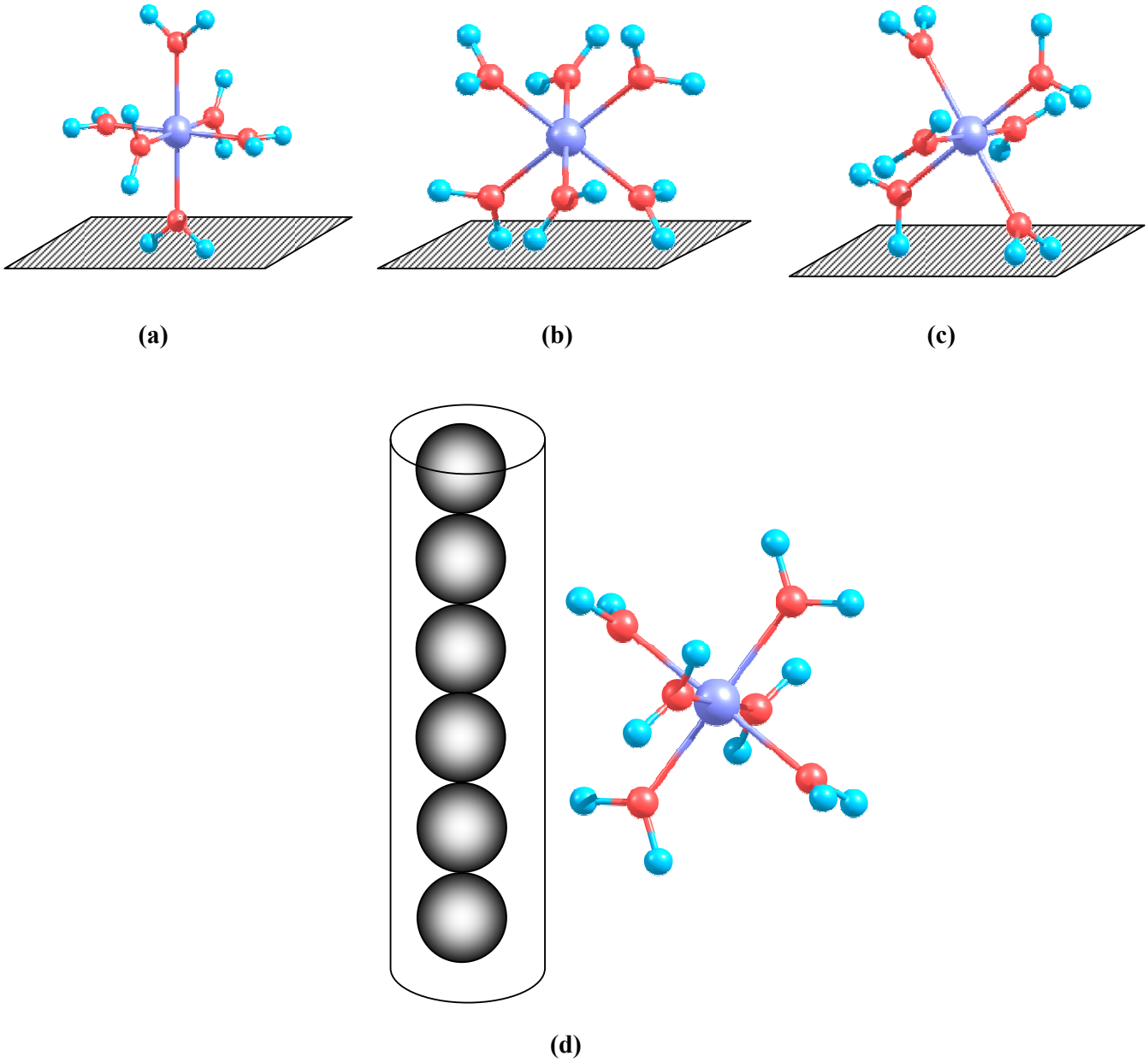

Figure 1. Selected orientations of the Fe(III) and Cr(III) aquacomplexes at the metal (111) surfaces: "apex"(**a**), "face" (**b**), "ridge" (**c**) and "ridge" at the monoatomic metal wires (**d**).

non-adiabatic character of electron transfer for a $Fe^{3+/2+}$ redox couple at the Au(111), Au(100) and Au(100) surfaces covered with a monolayer of Cu atoms was established in Refs.[27, 28], where the

matrix element V_{if} was calculated as a function of distance on the basis of the extended Hückel method. We found that in the non-adiabatic regime the nature of the metal significantly affects the electron transfer rate which leads to the following series of decreasing κ values: Pt > Au=Ag > Cu.

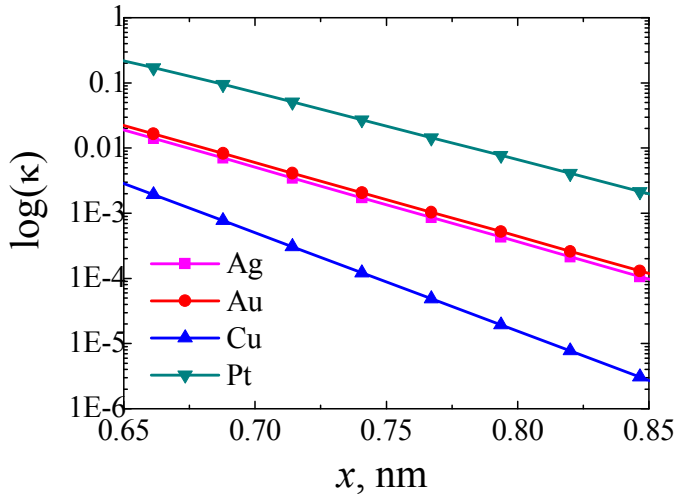

(**a**)

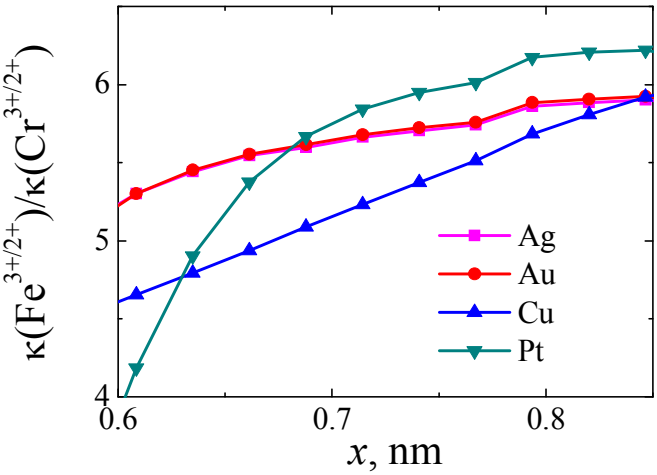

(**b**)

Figure 2. Electronic transmission coefficient vs separation calculated for reaction $[Fe(H_2O)_6]^{3+}$ + e = $[Fe(H_2O)_6]^{2+}$ at the (111) metal surfaces (**a**); ratio of electronic transmission coefficients vs separation characterizing redox couples $[Fe(H_2O)_6]^{3+/2+}$ and $[Cr(H_2O)_6]^{3+/2+}$ at the (111) metal surfaces (**b**)

Available experimental data on the influence of the electrode material on the rate constant (k) of the reduction (oxidation) of $Fe^{2+/2+}$ in aqueous solutions are contradictory. Bockris et al[29] have reported that k(Pt) > k(Au), while according to Angell and Dickinson results[30] the rate constants for the both electrodes are nearly the same. Figure 2b demonstrates the ratio of electronic transmission coefficients for $Fe^{3+/2+}$ and $Cr^{3+/2+}$ redox pairs for different electrodes. Electron transfer to $[Cr(H_2O)_6]^{3+}$ was found to be even more non-adiabatic as compared to Fe(III) aquacomplex; this could be attributed to the less diffuse character of the $[Cr(H_2O)_6]^{3+}$ acceptor orbital. Thus, our results agree qualitatively with experimental data for $Cr^{3+/2+}$ obtained by Weaver et al.[31]: k(Pt) > k(Au) > k(Ag). Note that the slope of the log(κ) vs x dependencies is steeper as compared with results obtained for other redox couples attached to the Au electrode through thiol tails of various lengths (see, for example, Refs.[32-34]). This difference might result mainly from a simplified construction of the effective wave function of a metal electrode from the total electronic density; the main contribution to the density comes from electrons of the *d*- band which are less diffusive than the electrons of *sp*-band. It is of worth to mention here an interesting finding by Gosavi and Marcus[14, 15]: because of competing roles of *d*- and *sp*- metal electrons, in general the rate constant is a sum of channels for each type of electrons, and the rate constant is not proportional to the total $\rho(\varepsilon_F)$, as illustrated specifically for Pt and Au.

The difference in orbital overlap effects between two metal slabs and monoatomic wires for the both redox pairs is shown in Figure 3. Two intervals of x can be distinguished for Cu, Au and Pt: "a catalytic" region, where κ(wire) > κ(Me slab) and "an inhibition" region, where κ(wire) < κ(Me slab). The stronger the orbital overlap, the more noticeable is the catalytic properties of the metal wires. For the silver nano-wire a slight catalytic effect is observed, which practically does not depend on distance. As the κ values for $[Cr(H_2O)_6]^{3+/2+}$ were found to be smaller than for $[Fe(H_2O)_6]^{3+/2+}$, the metal wires induce mostly "inhibition" effect for $Cr^{3+/2+}$ redox couple (Fig.3b).

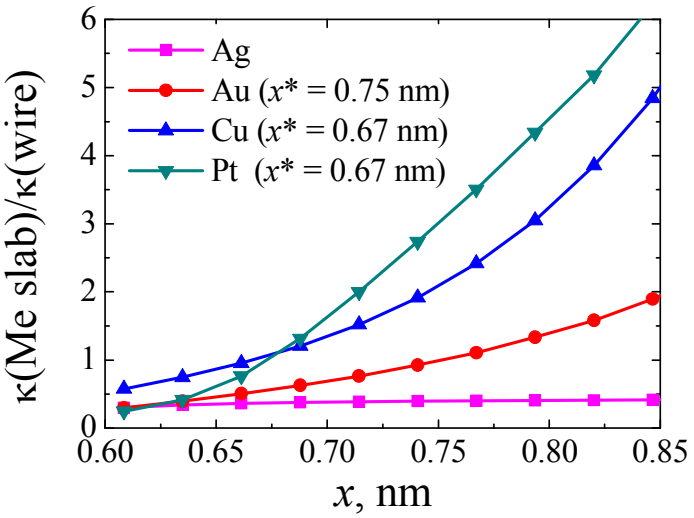

(**a**)

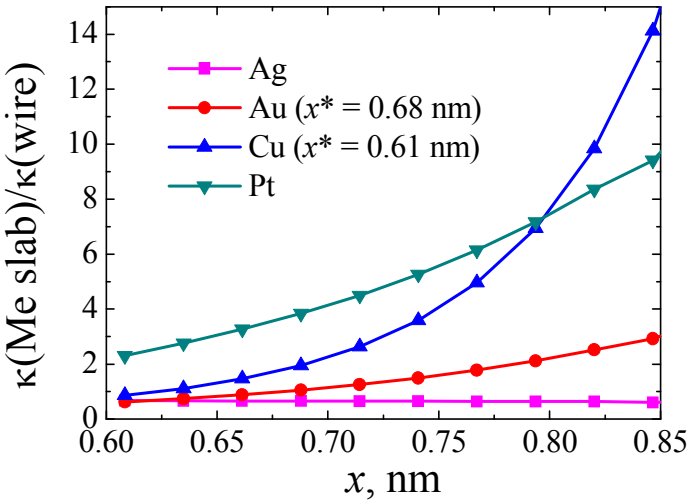

(**b**)

Figure 3. Ratio of electronic transmission coefficients vs separation characterizing redox couple $[Fe(H_2O)_6]^{3+/2+}$ (**a**) and $[Cr(H_2O)_6]^{3+/2+}$ (**b**) at the (111) metal surfaces and at the monoatomic wires; point x^* separates "catalytic" (κ(wire) > κ(Me slab)) and "inhibition" (κ(wire) < κ(Me slab)) regions.

To reinforce this important conclusion, we also calculated the squared matrix element (coupling constant) extracted from the computational data reported in Ref.[7] on the adsorption of a hydrogen atom at the Au(111) surface (hollow site) and at the monoatomic Au wire, where the Volmer step of hydrogen evolution reaction was investigated. Note that the coupling constant was estimated indirectly by fitting the electronic density of states projected to the adsorbed H atom. The results are exhibited in Figure 4. The catalytic activity of the metal wire at short distances can be clearly distinguished also for significantly adiabatic electron transfer (strong coupling limit). However, starting from a certain distance the catalytic properties of the metal wire disappear and the "inhibition" region takes place.

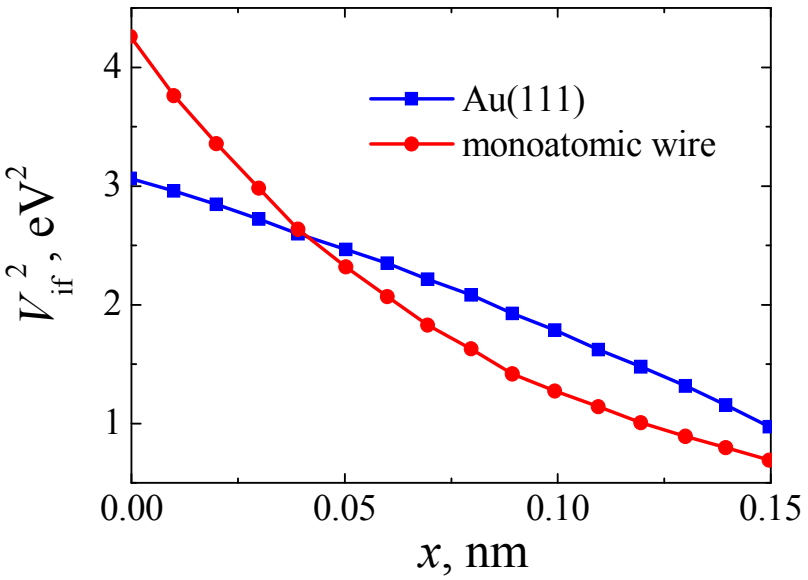

Figure 4. Coupling parameter vs distance calculated for the adsorption of a hydrogen atom on the Au(111) surface (hollow site) and a monoatomic golden wire; x is calculated from the Me – H equilibrium distance in adsorbed state.

IV. Concluding remarks

We have explored the orbital overlap effect on outer-sphere electron transfer across Me(111) and monoatomic metal wire/electrolyte solution interface. The Cu, Au and Pt wires (except Ag)

reveal catalytic activity at short distances and "inhibition" region for larger separations. Our method is based on a quantum mechanical theory combined with DFT for periodic systems and molecules. Although some molecular level details of the reaction layer were neglected (first of all, microscopic description of solvent molecules), the approach seems to be robust and makes it possible to predict some effects of qualitative nature. We considered the limiting case (the monoatomic metal wires), however, our analysis can be readily extended to cylindrical wires of arbitrary diameter; simple models based on the free electron gas concept can be employed to develop interpolation schemes (see, for example, Ref.[35]).

A shortcoming of the present work is obviously a possible experimental verification of the model predictions. Although a number of various electrochemical systems of nanosize were already probed using different experimental technique (see, e.g. Refs. cited in works[3, 9]), the authors investigated the averaged properties of arrays of carbon nanotubes and metal nanowires. Reliable kinetic measurements on a single nanosize electrode remain still an exceedingly complicated and challenging problem. Nevertheless, recent experimental results reported by the authors of Refs.[36, 37] look inspiring. In these works some electron transfer reactions at individual metal nanowires and single –walled carbon nanotubes in electrolyte environment were studied using voltammetry. The thickness of nanowires in the experiments[36, 37] ranged in the interval 32 – 110 nm but we believe that relevant data obtained for metal wires of smaller diameter will be available in the nearest future. Anyway possible applications of catalysis on metal nanowires in practice are very tempting.

Acknowledgement

This work was supported in part by the RFBR (project № 11-03-01186-a) and DFG. Financial support by the DFG (Schm 344/40-1) is gratefully acknowledged. We also thank Galina Tsirlina for helpful discussions.

Supporting information available: This material is available free of charge via the Internet at http://pubs.acs.org.

References

(1) Leiva, E.P.M.; Sánchez, C.G.; Vélez, P.; Schmickler, W. Theory of Electrochemical Monoatomic Nanowires. *Phys. Rev.B.* **2006**, *74*, 035422-035428.

(2) Henstridge, M.C.; Dickinson, E.J.F.; Compton, R.G. On the Estimation of the Diffuse Double Layer of Carbon Nanotubes Using Classical Theory: Curvature Effects on the Gouy–Chapman Limit. *Chem. Phys. Lett*. **2010**, *485*, 167-170.

(3) Nazmutdinov, R.R.; Bronshtein, M.D.; Schmickler, W. Electron Transfer Across a Conducting Nanowire (Nanotube)/Electrolyte Solution Interface. *Electrochim. Acta*. **2009**, *55*, 68-77.

(4) Frank, S.; Hartnig, C.; Groβ, A.; Schmickler, W. Spiral Adsorbate Structures on Monoatomic Nanowire Electrodes. *Chem. Phys. Chem*. **2008**, *9*, 1371-1374.

(5) Frolov, A.I.; Fedorov, M.I.; Rozhin, A.G. Ion Interactions with the Carbon Nanotube Surface in Aqueous Solutions: Understanding the Molecular Mechanisms. *Chem. Phys. Chem*. **2010**, *11*, 2612-2616.

(6) Heller, I.; Kong, J.; Williams, K.A.; Dekker, C.; Lemay, S.G. Electrochemistry at Single-Walled Carbon Nanotubes: The Role of Band Structure and Quantum Capacitance. *J. Am. Chem. Soc*. **2006**, *128*, 7353-7359.

(7) Santos, E.; Quaino, P.; Soldano, G.; Schmickler, W. Electrochemical Reactivity and Fractional Conductance of Nanowires. *Electrochem. Comm*. **2009**, *11*, 1764-1767.

(8) Soldano, G.; Santos, E.; Schmickler, W. Intrinsic Stability and Hydrogen Affinity of Pure and Bimetallic Nanowires. *J. Chem. Phys*. **2011**, *134*, 174106-174113.

(9) Nazmutdinov, R.R.; Berezin, S.A.; Soldano, G.; Schmickler, W. Bond Breaking Electron Transfer Across a Conducting Nanowire (Nanotube)/Electrolyte Solution Interface: The Role of Electrical Double Layer Effects. *J. Electroanal. Chem*. **2011**, *660*, 309-313

(10) Kuznetsov, A.M. *Charge transfer in physics, chemistry and biology: The physical mechanism of elementary processes and introduction to the theory*, Gordon and Breach, 1995.

(11) Kuznetsov, A.M.; Nazmutdinov, R.R.; Schmickler, W. Monte Carlo Simulations of Electrochemical Electron Transfer Processes. *J. Electroanal. Chem*. **2002**, *532*, 171-180.

(12) Brenemann, C.M.; Wiberg, K.B. Determining Atom-Centered Monopoles From Molecular Electrostatic Potentials. The Need for High Sampling Density in Formamide Conformational Analysis. *J. Comput. Chem*. **1990**, *11*, 361-373.

(13) Gao, Y.Q.; Marcus, R.A. On the Theory of Electron Transfer Reactions at Semiconductor/ Liquid Interfaces. II. A Free Electron Model. *J. Chem. Phys*. **2000**, *113*, 6351-6360.

(14) Gosavi, S.; Marcus, R.A.. Nonadiabatic Electron Transfer at Metal Surfaces. *J. Phys. Chem. B*. **2000**, *104*, 2067-2072.

(15) Gosavi, S.; Marcus, R.A. Temperature Dependence of the Electronic Factor in the Nonadiabatic Electron Transfer at Metal and Semiconductor Electrode. *J. Electroanal. Chem*. **2001**, *500*, 71-77.

(16) Gaussian 03, Revision B.04, M. J. Frisch , G. W. Trucks, H. B. Schlegel, G. E. Scuseria et al.

(17) Hammer, B.; Hansen, L.B.; Nørskov, J.K. Improved Adsorption Energetics Within Density-Functional Theory Using Revised Perdew-Burke-Ernzerhof Functionals. *Phys. Rev. B*. **1999**, *59*, 7413-7421.

(18) Monkhorst, H.J.; Pack, J.D. Special Points for Brillouin-Zone Integration. *Phys. Rev. B*. **1976**, *13*, 5188-5192.

(19) Perdew, J.P.; Burke, K.; Ernzerhof, M. Generalized Gradient Approximation Made Simple. *Phys. Rev. Lett*. **1996**, *77*, 3865-3868.

(20) Vanderbilt, D. Soft Self-Consistent Pseudopotentials in a General Eigenvaue Formalism. *Phys. Rev. B*. **1990**, *41*, 7892-7895.

(21) Kornyshev, A.A.; Kuznetsov, A.M.; Ulstrup, J. Effect of Overpotential on the Electronic Tunnel Factor in Diabatic Electrochemical Processes. *J. Phys. Chem*. **1994**, *98*, 3832-3837.

(22) Nazmutdinov, R.R.; Glukhov, D.V.; Tsirlina, G.A.; Petrii, O.A. Activationless Reduction of the Hexacyanoferrate Anion on a Mercury Electrode. *Russ. J. Electrochem*. **2003**, *39*, 97-107.

(23) Nazmutdinov, R.R.; Rusanova, M.Yu.; VanderPorten, D.; Tsirlina, G.A.; Fawcett, W.R. Towards the Reactivity Prediction: Outersphere Electroreduction of Transition-Metal Ammine Complexes. *J. Phys. Chem.* ***C***. **2009**, *113*, 2881-2890.

(24) Smith, J.R. Self-Consistent Many-Electron Theory of Electron Work Functions and Surface Potential Characteristics for Selected Metals. *Phys. Rev*. **1969**, *181*, 522-529.

(25) Rosso K.M.; Rustad, J.M. Ab Initio Calculation of Homogeneous Outer Sphere Electron Transfer Rates: Application to $M(OH_2)_6^{3+/2+}$ Redox Couples. *J. Phys. Chem. A*., 2000, *104*, 6718-6725.

(26) Nazmutdinov, R.R. Quantum Chemical Description of Charge Transfer Processes at the Metal/Solution Interface: Yesterday, Today, Tomorrow. *Russ. J. Electrochem*. **2002**, *38*, 111-122.

(27) Curtiss, L.A.; Halley, J.W.; Hautman, J.; Hung, N.C.; Nagy, Z.; Rhee, Y.-J. Yonco, R..M. Temperature Dependence of the Heterogeneous Ferrous-Ferric Electron Transfer Reaction Rate: Comparison of Experiment and Theory *J. Electrochem. Soc*. **1991**, *138*, 2032-2040.

(28) Nagy, Z.; Curtiss, L.A.; Hung, N.C.; Zurawski, D.J.; Yonco, R.M. Catalytic Effect of Under-Potential Deposited Layers on the Ferrous/Ferric Outer-Sphere Electrode Reaction. *J. Electroanal. Chem*. **1992**, *325*, 313.

(29) Angell, D.H; Dickinson, T. The Kinetics of the Ferrous/Ferric and Ferro/Ferricyanide Reactions at Platinum and Gold Electrodes: Part I. Kinetics at Bare-Metal Surfaces. *J. Electroanal. Chem*. **1972**, *35,* 55-72.

(30) Bockris, J.O"M.; Mannan, R.J.; Damjanovic, A. Dependence of the Rate of Electrode Redox Reactions on the Substrate. *J. Chem. Phys*. **1968,** *48*, 1898-1904.

(31) Barr, S.W.; Guyer, K.L.; Weaver, M.J. The Dependence of the Kinetics of Some Simple Outer-Sphere Electrode Reactions on the Nature of the Electrode Material. *J. Electroanal. Chem*. **1980**, *111*, 41-59.

(32) Smalley, J.F.; Finklea, H.O.; Chidsey, E.E.D.; Linford, M.R.; S.E. Creager, Ferraris, J.P.; Chalfant, K.; Zawodzinsk, T.; Feldberg, S.W.; Newton, M.D. Heterogeneous Electron-Transfer Kinetics for Ruthenium and Ferrocene Redox Moieties through Alkanethiol Monolayes on Gold. *J. Am. Chem. Soc*. **2003**, *125*, 2004-2013.

(33) Newton, M.D.; Smalley, J.F. Interfacial Bridge-Mediated Electron Transfer: Mechanistic Analysis Based on Electrochemical Kinetics and Theoretical Modeling. *Phys. Chem. Chem. Phys*. **2007**, *9*, 555-572.

(34) Khoshtariya, D.E.; Dolidze, T.D.; Zusman, L.; Waldeck, D.H. Observation of the Turnover Between the Solvent Friction (Overdamped) and Tunneling (Nonadiabatic) Charge Transfer Mechanisms for a Au/$Fe(CN)_6^{3-/4-}$ Electrode Process and Evidence for a Freezing Out of the Marcus Barrier. *J. Phys. Chem. A*. **2001**, *105*, 1818-1829.

(35) Bruzzone, S.; Arrighini, G.P.; Guidotti, C. Some Spectroscopic Properties of Gold Nanorods According to a Schematic Quantum Model Founded on the Dielectric Behavior of the Electron-Gas Confined in a Box. *Chem. Phys*. **2003**, *291*, 125-140.

(36) Dudin, P.V.; Snowden, M.E.; Macpherson, J.V.; Unwin, P.R. Electrochemistry at Nanoscale Electrodes: Individual Single-Walled Carbon Nanotubes (SWNTs) and SWNT-Templated Metal Nanowires. *ACS. NANO*. **2011**, *5*, 10017-10025.

(37) Dawson, K.; Wahl, A.; Murphy, R.; O'Riordan, A. Electrocatalysis at Single Gold Nanowire Electrodes. *J. Phys. Chem. C*. **2012**, *116*, 14665-14673.

Graphical abstract

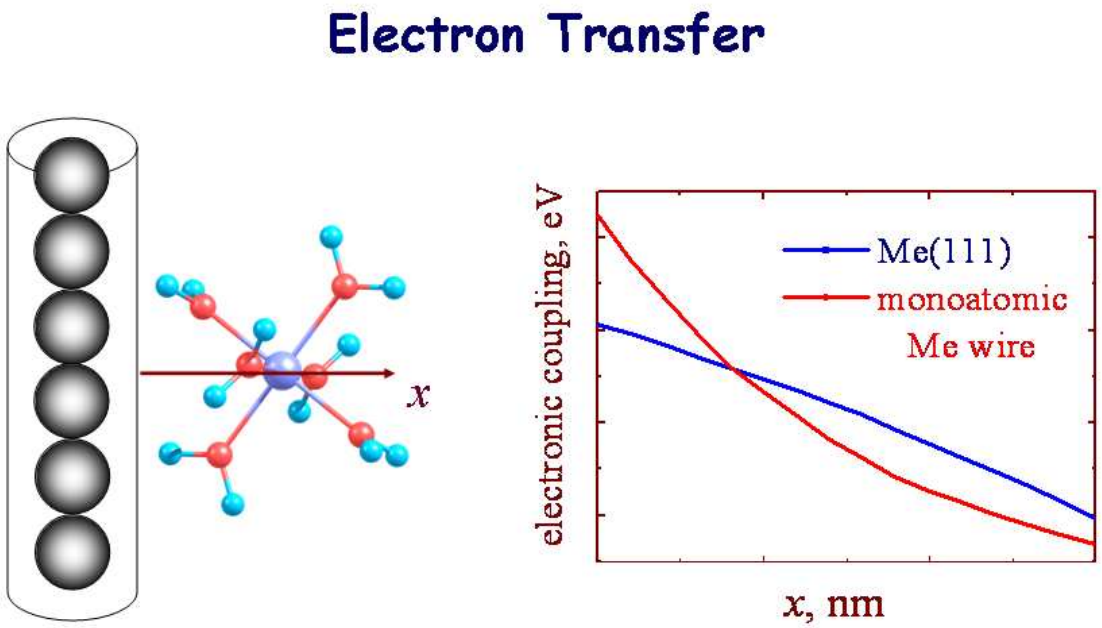

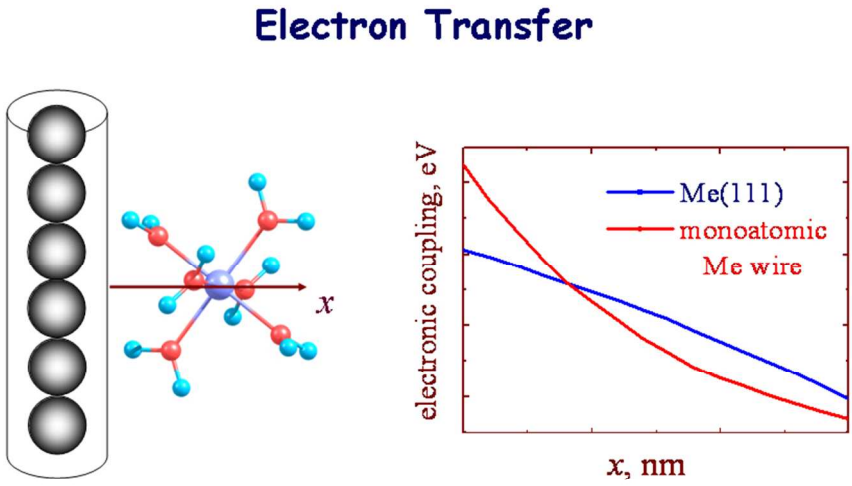

254x190mm (96 x 96 DPI)